RSC Advances

ROYAL SOCIETY OF CHEMISTRY

www.rsc.org/advances

Journal Name

ARTICLE

Temperature-Responsive Zinc Oxide Nanorods Arrays Grafted with Poly(*N*-isopropylacrylamide) via SI-ATRP

Received 00th January 20xx,
Accepted 00th January 20xx

DOI: 10.1039/x0xx00000x

www.rsc.org/

Qian Feng, Dongyan Tang,* Haitao Lv, Weile Zhang and Wenbo Li

Well fabricated ZnO nanorods (ZnO NRs) arrays with preferred-orientation that grown on pre-deposited ZnO seed layers substrate were selected to graft thermo-responsive polymers of poly(*N*-isopropylacrylamide) (PNIPAM) by surface-initiated atom transfer radical polymerization (SI-ATRP). As a controlled/"living" radical polymerization, SI-ATRP could endow the systems with the characteristics of the grafted PNIPAM, meanwhile, with the maintaining of the properties of ZnO nanorods. The structures of ZnO and the grafted polymer with the relative high molecular weights (*Mn*, 24300) and narrow molecular weight distributions (*Mw/Mn*, 1.19) that determined by GPC detection, were characterized by XRD and FT-IR. The graft amount of PNIPAM on ZnO nanorods and the interactions between the two components were determined by TG and XPS, respectively. The relative thin layers of PNIPAM (~15 nm) formed around NRs via SI-ATRP method were observed by SEM. And the temperature-sensitivity of the grafted nanorods were proved by the contact angles measurements. Furthermore, photodegradation of Rhodamine B (Rh-B) by the grafted nanorods revealed that ZnO NRs-PNIPAM exhibited photocatalysis and temperature responsibility characteristics, indicating the significant potential applications with tunable responsiveness by changing the environmental conditions.

Introduction

ZnO, with a wide large band gap of 3.37 eV at 300 K and a large excitation binding energy of 60 meV,[1,2] has been considered as an excellent multifunctional semiconductor candidate.[3-5] Different morphologies of ZnO nanostructures have salient effects on their properties and applications.[6-8] In particular, the large surface-to-volume ratio, direct carrier conduction path and the efficiency of the exaction recombination[9] in nanorods of ZnO (ZnO NRs) make them ideal for sensors,[10] light emitting diodes,[11] optoelectronic devices,[12] dye-sensitized solar cells,[13] antibacterial agents,[14] *etc*.

To expand the field of applications of ZnO nanostructures and to mitigate shortcomings such as poor solubility in aqueous medium, bad biocompatibility and easy agglomeration of nanoparticles, a number of groups have investigated organic/inorganic nanocomposites combining the optical, electronic, and mechanical properties of the inorganic nanorods with the solubility, mechanical and chemical stability of organic polymers. Yang *et al*.[15] designed a novel sandwich-structured UV photodetector composed of polyaniline nanowires and ZnO nanorods, which only need UV light as power source. Wu *et al*.[16] fabricated 10,12-pentacosadiynoic acid (PCDA)/ZnO composites and demonstrated a colorimetric change with the increase of ZnO concentrations. Among these ZnO based nanocomposites related researches, considering the untunable performance of ZnO or any other restrictions on the applications of semiconductor materials, efforts on the modification of ZnO nanostructures with functions (such as stimuli-responsive), organic components have received much more considerable attentions.

Stimuli-responsive smart polymers have great potentials in many areas due to their remarkable responsive behaviors in response to external stimuli, *e.g.* temperature, *pH*, magnetic field and light.[17] So it is expected that organic/inorganic nanocomposites would present the tunable property by incorporating stimuli-responsive polymers into. Of the many environmentally sensitive polymers, poly(*N*-isopropylacrylamide) (PNIPAM), is used most extensively in the functional textiles, intelligent microfluidic, controlled drug release, and thermally responsive filters.[18] With a lower critical solution temperature (LCST) in aqueous solution between 30 and 35 ^{0}C, PNIPAM could display reversible switchable behaviors between the hydrophilicity and hydrophobicity depending on its detailed structures.[19] Hou *et al*.[20] prepared self-assembled graphene-PNIPAM hydrogels with a 3D network structure using a hydrothermal method to exhibit good electrical conductivity, high mechanical strength and reversible stimulus-sensitive volume changes. Chen *et al*.[21] synthesized photoelectrode nanocomposites by the incorporation of TiO_2 nanoparticles with *pH*-stimuli responsive polymer and found that their photocurrent behavior was tunable in response to *pH*-stimuli.

Relative to the traditional techniques to obtain nanocomposites, such as blending, *in situ* polymerization, atomic layer deposition (ALD) and self-assembly,[22-25] SI-ATRP

Department of Chemistry, School of Science, Harbin Institute of Technology, Harbin 150001, China

could precisely control the molecular characteristics of polymer chains tethered to nanoparticle surfaces and provide a densely packed array of polymer chains to engineer the structure and properties of polymer/inorganic interfaces.[26,27] As a controlled/"living" radical polymerization, ATRP exhibits better controlling over the chain lengths, and accordingly, the thickness of the grafted polymers.[28,29] Such surface modification via SI-ATRP could maintain the properties of semiconductor materials and introduce the surface properties of the grafted polymers. Benjamin *et al*.[30] modified the surface of ZnO nanowires with a variety of polymers, such as poly(methylmethacrylate) and polystyrene, by ATRP and analyzed the grafting density of the surface initiators. Xu *et al*.[31] synthesized magnetic ZnO surface-imprinted polymers by SI-ATRP and demonstrated the potential applications in the recognition and separation of antibiotics.

Herein, we provided a practical and flexible approach to modify ZnO NRs with temperature-stimuli responsive PNIPAM via SI-ATRP method and further investigated their temperature-dependent photocatalytic behaviors. The results revealed that ZnO NRs-PNIPAM still maintained photocatalysis and temperature responsibility, indicating the significant potential for using coating with tunable, environmentally responsive phase transformations.

Experimental

Materials

N-Isopropylacrylamide (NIPAM, 98.0%), was purchased from Tokyo Chemical Industry (Tokyo, Japan) and used without further purification. 3-Aminopropyltriethoxysilane (APTES, 99.0%), 2-bromoisobutyryl bromide (BiBB, 98.0%), copper(I) bromide (CuBr, 99.0%), and N,N,N',N'',N''-pentamethyldiethylenetriamine (PMDETA, 99.0%) were all obtained from Aladdin (Beijing, China) and used directly. Ethanol, ammonia, triethanolamine (TEA), toluene were all purchased from Sinopharm Reagent Co., Ltd (Beijing, China). Ultrapure water was purified by a KSV Minitrough system (~18.2 MΩ cm).

Deposition of ZnO Nanorods and the amino-functionalization.

Well-orientated ZnO NRs were prepared by a two-step method including pre-deposition of seed layers of ZnO onto the substrate by LB method and the following hydrothermal process of ZnO nanorods onto the seed layers, as reported earlier.[32]

Then the ZnO NRs were immersed in a mixture of ethanol (50 mL) and ammonia solution (50 μL). APTES (0.4 mL, 1.7 mmol) was added dropwise and then stirred at 60 ^{0}C for 12 h. The amino-functionalized ZnO NRs were rinsed with ethanol to remove the remaining ATPES and then dried in a vacuum at 70 ^{0}C overnight.

Synthesis of BiBB-Functionalized ZnO Nanorods.

The above amino-functionalized ZnO NRs were added to BiBB (0.4 mL, 3.2 mmol) in a mixture of toluene (50 mL) and TEA (0.45 mL, 3.2 mmol) at 0 ^{0}C with the constant stirring for 1 h. Then, the mixture was allowed to warm to room temperature and stirred overnight. The BiBB-Functionalized ZnO NRs were cleaned with toluene, and dried in a vacuum oven overnight at 70 ^{0}C.

Grafting of PNIPAM on the Surface of ZnO Nanorods by SI-ATRP (represented as ZnO NRs-PNIPAM).

SI-ATRP of NIPAM was carried out by immersing the BiBB-functionalized ZnO NRs in a Schlenk flask containing NIPAM (0.7 g, 6.2 mmol), PMDETA (75 μL, 0.4 mmol), and ultrapure water (20 mL). The mixture was degassed by one freeze-pump-thaw cycle. During the frozen state, CuBr (20 mg, 0.14 mmol) was added under the flowing N_2. The flask was then subjected to two additional freeze-pump-thaw cycles. To start the reaction, it was warmed to room temperature under nitrogen.[33] After 6h at room temperature, the obtained ZnO NRs-PNIPAM were rinsed thoroughly with ultrapure water and dried in a vacuum oven overnight at 70 °C. The obtained samples were treated with hydrofluoric acid to liberate the grafted PNIPAM chains for further analysis.

The general approaches of the synthesis of amino-functionalized, BiBB-functionalized ZnO NRs, and the preparation of ZnO NRs-PNIPAM were shown in Scheme 1.

Characterization

Infrared spectra were collected on a FT-IR spectrometer (FT-IR, AVATER-360B, Nicolet, USA) in the range from 1000 cm^{-1} to 4000 cm^{-1}.

X-ray diffractometer analyses were performed on the D/max-γB X-ray diffractometer (XRD, Rigaku, JP) using Cu Kα radiation in the 2ϑ range of 30–60 ^{0} at a voltage of 45 kV and a current of 35 mA.

Molecular weights and molecular weight distributions were determined by a gel permeation chromatograph (GPC, Water, USA) equipped with a Water 1515 pump and a Water 2414 differential refractive index detector. Polystyrene was used as a calibration standard and *N,N'-dimethylformamide* as the eluent with a flow rate of 1.0 mL · min^{-1}.

Surface elemental compositions of ZnO NRs and ZnO NRs-PNIPAM nanocomposites, and the interactions between the two components were characterized and analyzed using X-ray photoelectron spectroscopy (XPS, PHI-5700, Physical Electronics Co., USA) employing an Al Kα X-ray resource (1486.6 eV) and a concentric hemispherical energy electron analyzer operating at 12.5 kV and 250 W with a chamber pressure of 10^{-6} Torr.

Thermogravimetric analyses were carried out to investigate the graft density of PNIPAM onto the surface of nanorods at a heating rate of 10 ^{0}C · min^{-1} from room temperature to 800 ^{0}C using thermogravimetric analyze (TG, Pyris 6, Perkin-Elmer, USA).

The morphologies of ZnO NRs and ZnO NRs-PNIPAM nanocomposites were observed by a scanning electron microscope (SEM, HELIOS NANOLAB 600i, FEI, USA).

Thermo-Responsive Behavior and Photocatalytic Ability

Contact angles were measured by the sessile drop method at 25 and 45 ^{0}C on a contact angle goniometer (CA, JC-200,

Shanghai Solon Information Technology, CN) to perform the thermosensitivity of ZnO NRs-PNIPAM nanocomposites. Typically, three drops of the water were placed on the surface of the samples and three readings of the contact angles were taken for each drop. The average of nine readings was used as the final contact angle of each sample. The injection volume was about 2 μL.

The degradation experiments of rhodamine B (Rh-B) aqueous solution (10 mg L^{-1}, 30 mL, *pH*=7) under UV-light were employed at 25 and 45 ^{0}C to evaluate the photocatalytic abilities of ZnO NRs-PNIPAM nanocomposites. Equilibrium experiments were first carried out for the two pieces of nanocomposites with the same size (3.0 mg) for 12.0 h to reach adsorption/adsorption equilibrium. The photocatalytic efficiency was calculated by the equation of $D = (C_0 - C_t)/C_0$, where D referred to the degradation ratio, C_0 and C_t referred to the concentrations of Rh-B solution before and after the irradiation. The concentrations of Rh-B were detected by UV-Vis spectrophotometer (UV-Vi, Beijing Purkinje General Instrument, 760CRT, CN). For comparison, the same method was used for the degradation of Rh-B aqueous solution in the presence of ZnO NRs.

Results and discussions

Materials characterization

FT-IR spectrum of the modified ZnO NRs at various stages are shown in Fig. 1(a) to (d). The strong peaks at 460 cm^{-1} was assigned to the characteristic peak of ZnO[34] in Fig. 1(a)-(d) and the absorption peaks at 3400 cm^{-1} corresponded to hydroxyl groups on ZnO NRs in Fig. 1(a). In Fig. 1(b), the new absorption at 1620.1 cm^{-1} from the amino group could be observed, indicating successful surface modification of ZnO NRs.[35] In Fig. 1(c), new peaks from the 2-bromoisobutyramide at 3571, 3384, 1633, 1534, 1475 and 1376 cm^{-1} demonstrated that the SI-ATRP initiator had successfully been installed on the surface of the spectra of BiBB-functionalized ZnO NRs. The strong absorption peaks at 1650 (C=O stretching) and 1540 cm^{-1} (N-H bending), and 1460 and 1390 cm^{-1} (C-H bending) as shown in Fig. 1(d), confirmed the successful graft of PNIPAM via SI-ATRP on the ZnO NRs surfaces.[19]

Fig. 2 displayed the XRD pattern of ZnO NRs and ZnO NRs-PNIPAM nanocomposites. The peaks located at 2ϑ of 31.68 ^{0}, 34.48 ^{0}, 36.22 ^{0}, and 47.52 ^{0} were indexed to (100), (002), (101), (102), and (103) diffractions of ZnO, respectively (JCPDS 36−1451) in curve (a) of Fig. 2. As shown in curve (b) of ZnO NRs-PNIPAM nanocomposites in Fig 2, these characteristic peaks also existed, indicating the structures of NRs were unchanged by the SI-ATRP polymerization. Compared with the XRD pattern of ZnO NRs (a), the intensities of all the peaks of ZnO NRs-PNIPAM in curve (b) were in less strengths. Owing to the encapsulation of ZnO nanorods, active sites on the surface of NRs were coated by PNIPAM partially, resulting the decline of the above mentioned characteristic peaks.[36]

The grafted PNIPAM chains were liberated from ZnO NRs-PNIPAM nanocomposites for GPC analysis by treating with hydrofluoric acid. The time evolution of number average molecular weights (*Mn*), and molecular weight distributions (*Mw/Mn*) for the cleaved PNIPAM chains, is shown in Fig. 3. After 6 h, the PNIPAM had reached *Mn* of 24300 Daltons and a molecular weight distribution (*Mw/Mn*) of 1.19. The small shoulder appeared in the figure might result from the impurities or lower molecular weight components. The GPC results exhibited a relative narrow molecular weight distribution of PNIPAM (around the value of 1.0) on ZnO nanorods by controlled/living radical polymerization for our present synthesized procedures.

The wide-scan, N1s, Zn2p and Br3d XPS spectra of ZnO NRs-BiBB and ZnO NRs-PNIPAM nanocomposites were shown in Fig. 4(a), (b) and (c), respectively. Table 1 showed the element concentration calculated from the XPS detection results. The atomic concentration of C and N in the ZnO NRs-PNIPAM nanocomposites increased from 35.04 to 78.16 % and from 1.13 to 8.77 % respectively, while the atomic concentration of O element decreased from 19.14 to 9.83 %. This change in C, N and O concentrations on the surface of ZnO nanorod were consistent with surface grafting of PNIPAM. Br element in Fig. 4(d) confirmed the present of the ATRP initiators of BiBB on the surface of ZnO NRs.[37] Decrease in Zn from 9.40 to 2.24 % indicated some active sites remained even after surface modification of the ZnO NRs-PNIPAM. SI-ATRP at present work supplied an effective grafting method for polymers with different functional on the surface of the inorganic phase, without sacrificing its original properties.[38]

Furthermore, the software of XSPEAK 4.1 was employed to fit the C1s peak of ZnO NRs-PNIPAM (as shown in Fig. 5). The three sub-peaks corresponded hydrocarbon (C_xH_y: 285.5 eV), carbon adjacent to an amide group (C-C=O: 286.4 eV), and carbon attached to oxygen and nitrogen (N-C=O: 288.2 eV), respectively.[39] The appearance of the three peaks for carbon proved the success grafting of PNIPAM onto ZnO NRs by SI-ATRP method.

The grafting amount of the initiator and PNIPAM on the surface of ZnO NRs could be measured by TG analysis.[40] Fig. 6 displayed the decomposition behavior of ZnO NRs, ZnO NRs-BiBB and ZnO NRs-PNIPAM under nitrogen atmosphere at different temperatures by TG detections. ZnO NRs showed a weight loss of about 4.90% as heating from 50 to 780 ^{0}C in the curve (a), due to the removal of the absorbed water and the decomposition of the hydroxide group. TGA revealed 2.99 wt % difference in weight retention at 780 ^{0}C between ZnO NRs and ZnO NRs-BiBB in the curve(a) and (b), attributed to the degradation of organic components from the grafted initiator on the surface of ZnO NRs, indicating that the grafting amount of the initiator groups on the surface of ZnO NRs was roughly estimated to be 0.100 mmol g^{-1} calculated by the method in a previous report.[41] As shown in the curve(c) in Fig. 6, the weight retention at 780 ^{0}C obtained for ZnO NRs-PNIPAM nanocomposites was 73.77 %. Using the weight retention at 780 ^{0}C of ZnO NRs-BiBB in curve (b) as a reference, the weight content of the grafting polymers was calculated to be 18.34 %, indicating the presence of polymer on the surfaces of ZnO NRs. The purpose of this work focused on providing a practical and

flexible approach to prepare ZnO NRs-PNIPAM with better photocatalysis performance, as well as temperature responsivity. Too much polymer coated on the NRs would occupy the active sites onto the surfaces of ZnO NRs and sacrificing its original properties. Therefore, it was well demonstrated that PNIPAM molecule chain had been successfully grafted onto ZnO NRs by SI-ATRP method, in agreements with that of the XPS measurement results of C1s peak of ZnO NRs-PNIPAM, as shown in Fig. 5.[42]

Fig. 7 displayed the morphologies of ZnO NRs and ZnO NRs-PNIPAM nanocomposites by SEM images. The unmodified ZnO NRs had smooth and clean surfaces with a typical hexagonal wurtzite strucutres shown in Fig. 7(a). These nanorods displayed high regularity and crystallinity, suggesting the better photocatalysis performance. In Fig. 7(b) and (c), after the SI-ATRP process to ZnO NRs, the smooth and regular surfaces became rough and their distinct edges changed to indistinct. These phenomena further confirmed the successful grafting of PNIPAM onto the surfaces of ZnO NRs. Compared with nanorods in Fig. 7(a) and (b), the contours of ZnO NRs-PNIPAM nanocomposites expanded and became indistinct due to the grafting of the polymers. Polymers coated on the surfaces of ZnO NRs would interfere the crystallinity of nanorods, indicating the reduction of the intensities of all the peaks of ZnO NRs-PNIPAM, that were in agreements with the XRD measurement results shown in Fig. 2. But the grafted ZnO NRs changed their original rod-like structures unobviously, indicating the existence of the characteristic peaks in XRD detections. Furthermore, the diameters of ZnO NRs in Fig. 7(b) were larger than those in Fig. 7(a), implying the formation of the thin layer of polymer with the thickness of approximately 15 nm.

Temperature-sensitive Behaviors

To study the temperature-sensitive behaviors of ZnO NRs-PNIPAM nanocomposites, Fig. 8 presented the CA values of the nanocomposites with the different contact times at 25 and at 45 ^{0}C, respectively. The values of angles decreased to 39.50 ^{0} with the increasing of contact time from 0-8 s at 25 ^{0}C, while there was no obvious changes at 45 ^{0}C with the CA values of 121.90 ^{0}. This phenomenon could be explained by the competition between the intermolecular and intramolecular hydrogen bond while below and above the LCST values of about 32 ^{0}C. Below the LCST, the predominantly intermolecular hydrogen bond between PNIPAM chains and water molecules contributed to the hydrophilicity of PNIPAM. Above the LCST, the intramolecular hydrogen bonding between C=O and N-H groups within PNIPAM chains resulted in a compact and collapsed conformation of PNIPAM chains, thus made it difficult for the hydrophilic C=O and N-H groups to interact with water molecules. Hence, seen from Fig. 8, this graft ZnO NRs exhibited temperature-sensitive variations between hydrophilicity and hydrophobicity with the changes of ambient temperatures. This enabled other functions to be added to the original properties of inorganic materials by surface modification.

Photocatalytic Behaviors Detections

Photocatalytic activity of ZnO NRs and ZnO NRs-PNIPAM nanocomposites were investigated through the degradation of Rh-B solution at 25 and 45 ^{0}C, respectively. Time-dependent absorption spectra of Rh-B solutions that under UV light (λ of 365 nm) illumination of ZnO-NRs at 25 ^{0}C (with *pH* of 7.0), ZnO NRs-PNIPAM nanocomposites at 25 ^{0}C (with *pH* of 7.0), and at 45 ^{0}C (with *pH* of 7.0) are shown in Fig. 9(a), (b) and (c). Under UV light illumination for 50 min, the absorption peak corresponding to Rh-B diminished with the time, indicating photocatalytsis of the ZnO NRs-PNIPAM prepared via SI-ATRP. Degradation ratios of Rh-B solution in the presence of ZnO NRs and ZnO NRs-PNIPAM nanocomposites at 25 and 45 ^{0}C were revealed in Fig. 10. For ZnO NRs, over 20% Rh-B could be degraded after 50 min of irradiation. A lower extent of Rh-B photodegradation could be obtained to about 14 % and 8.0 %, for the same irradiation time of ZnO NRs-PNIPAM nanocomposites at 25 and 45 ^{0}C, respectively. So, the photocatalytic efficiency of nanocomposites was much lower than that pure inorganic materials of ZnO NRs, owing mainly to the partial occupation of the active sites on the surface of NRs by SI-ATRP, and suggesting the decline of ZnO content. Whereas, the photocatalytic activity was higher for nanocomposites at 25 ^{0}C than that at 45 ^{0}C. These results could be reasoned that, at low temperature, the swelling of polymers made them more hydrophilic, and thus the chains of polymers were in a relaxed state.[43] The active sites could be exposed, and the Rh-B molecules thus could reach the surface of NRs easily. At higher temperature the collapsed PNIPAM chains block most of the active sites on the surface of NRs, reduction of their catalytic abilities (as illustrated in Scheme 2). Hence, grafting of stimuli-responsive polymer by SI-ATRP method to inorganic materials, as a feasible and promising method to fabricate valuable catalysis, could provide nanocomposites better responsibilities over surface modification and further the tunable catalytic properties.[36]

Conclusions

Surface-initiated atom transfer radical polymerization (SI-ATRP) was used to graft thermo-responsive PNIPAM onto the surfaces of ZnO nanorods (ZnO NRs) arrays with preferred-orientation, to afford a novel of ZnO NRs-PNIPAM nanocomposites photocatalysts. SI-ATRP ensured the grated PNIPAM on the surfaces of ZnO NRs with the relative high molecular weights, narrow molecular weight distributions PNIPAM on the surface of ZnO NRs without the sacrificing the active sites of ZnO NRs. The exposed active sites could enter into the photocatalytic reactions, the grafted polymer could endow ZnO NRs temperature responsivity characteristics. The photodegradation of Rhodamine B at lower temperature (25 ^{0}C) presented a significant catalysis than that at 45 ^{0}C. Moreover, functional PNIPAM grafted onto the surfaces of ZnO NRs could provide the nanocomposites tunable responsiveness by changing the environmental temperatures.

Acknowledgements

This work was supported by the National Natural Science Foundation of China (Grand No.51402073), the Fundamental Research Funds for the Central Universities and Program for Innovation Research of Science in Harbin Institute of Technology, China (No. T201410), and the Excellent Academic Leaders Foundation of Harbin, China (No. 2014RFXXJ017).

Notes and references

1 C. Klingshirn, *Phys. Status Solidi B*, 1975, **71**, 547.
2 Ü. Özgür, Ya. I. Alivov, C. Liu, A. Teke, M. A. Reshchikov, S. Doğan, V. Avrutin, S. J. Cho and H. Morkoç, *J. Appl. Phys.*, 2005, **98**, 041301–041404.
3 S. Q. Bi, F. L. Meng, Y. Z. Zheng, X. Han, X. Tao and J. F. Chen, *J. Power Sources*, 2014, **272**, 485–490.
4 D. Iqbal, A. Kostka, A. Bashir, A. Sarfraz, Y. Chen, A. D. Wieck and A. Erbe, *ACS. Appl. Mater. Interfaces*, 2014, **6**, 18728–18734.
5 S. K. Arya, S. Saha, J. E. Ramirez-Vick, V. Gupta, S. Bhansali and S. P. Singh, *Anal. Chim. Acta*, 2012, **737**, 1–21.
6 A. H. Jadhav, S. H. Patil, S. D. Sathaye and K. R. Patil, *J. Mater. Sci.*, 2014, **49**, 5945–5954.
7 S. L. Wang, X. Jia, P. Jiang, H. Fang and W. H. Tang, *J. Alloys Compd.*, 2010, **502**, 118–122.
8 K. K. Naik, R. Khare, D. Chakravarty, M. A. More, R. Thapa, D. J. Late and C. S. Rout, *Appl. Phys. Lett.*, 2014, **105**, 233101–233106.
9 R. S. Devan, R. A. Patil, J. H. Lin and Y. R. Ma, *Adv. Funct. Mater.*, 2012, **22**, 3326–3370.
10 P. Sanguino, T. Monteiro, S. R. Bhattacharyya, C. J. Dias, R. Igreja and R. Franco, *Sens. Actuators, B*, 2014, **204**, 211–217.
11 A. Echresh, C. O. Chey, M. Z. Shoushtari, O. Nur and M. Willander, *J. Appl. Phy.*, 2014, **116**, 193104–193112.
12 D. Sett, S. Sarkar and D. Basak, *RSC Adv.*, 2014, **4**, 58553–58558.
13 L. Z. Liu, Y. Q. Chen, T. B. Guo, Y. Q. Zhu, Y. Su, C. Jia, M. Q. Wei and Y. F. Cheng, *ACS. Appl. Mater. Interfaces*, 2012, **4**, 17–23.
14 R. Kumar, S. Anandan, K. Hembram and T. N. Rao, *ACS. Mater. Interfaces*, 2014, **6**, 13138–13148.
15 S. X. Yang, J. Gong and Y. L. Deng, *J. Mater. Chem.*, 2012, **22**, 13899–13902.
16 A. Wu, Y. Gu, C. Stavrou, H. Kazerani, J. F. Federici and Z. Iqbal, *Sens. Actuators, B*, 2014, **203**, 320–326.
17 M. R. Islam, Y. F. Gao, X. Li, Q. M. Zhang, M. L. Wei and M. J. Serpe, *Chin. Sci. Bull.*, 2014, **59**, 4237–4255.
18 J. Ramos, A. Imaz and J. Forcada, *Polym. Chem.*, 2012, **3**, 852–856.
19 H. G. Schild, *Prog. Polym. Sci.*, 1992, **17**, 163–249.
20 C. Y. Hou, Q. H. Zhang, Y. G. Li and H. Z. Wang, *Carbon*, 2012, **50**, 1959–1965.
21 D. Chen and J. H. Li, *J. Phys. Chem. C*, 2010, **114**, 10478–10483.
22 V. B. Schwartz, F. Thétiot, S. Ritz, S. Pütz, L. Choritz, A. Lappas, R. Förch, K. Landfester and U. Jonas, *Adv. Funct. Mater.*, 2012, **22**, 2376–2386.
23 Q. Y. Lu, J. J. Zhang, X. F. Liu, Y. Y. Wu, R. Yuan and S. H. Chen, *Analyst*, 2014, **139**, 6556–6562.
24 F. Kayaci, C. Ozgit-Alkgun, I. Donmez, N. Biyikli and T. Uyar, *ACS. Appl. Mater. Interfaces*, 2012, **4**, 6185–6194.
25 M. M. L. Arras, C. Schillai and K. D. Jandt, *Langmuir*, 2014, **30**, 14263–14269.
26 C. M. Hui, J. Pietrasik, M. Schmitt, C. Mahoney, J. Choi, M. R. Bockstaller and K. Matyjaszewski, *Chem. Mater.*, 2014, **26**, 745–762.
27 M. J. Mulvihill, B. L. Rupert, R. He, A. Hochbaum, J. Arnold and P. Yang, *J. Am. Chem. Soc.*, 2005, **127**, 16040–16041.
28 J. S. Wang and K. Matyjaszewski, *J. Am. Chem. Soc.*, 1995, **117**, 5614–5615.
29 K. Matyjaszewski and J. H. Xia, *Chem. Rev.*, 2001, **101**, 2921–2990.
30 B. L. Rupert, M. J. Mulvihill and J. Arnold, *Chem. Mater.*, 2006, **18**, 5045–5051.
31 L. C. Xu, J. M. Pan, J. D. Dai, Z. J. Cao, H. Hang, X. X. Li and Y. S. Yang, *RSC Adv.*, 2012, **2**, 5571–5579.
32 Q. Feng, D. Y. Tang, E. Y. Jing, S. Gu and S. Han, *J. Alloys Compd.*, 2013, **578**, 228–234.
33 T. Wu, Z. S. Ge, S. Y. Liu, *Chem. Mater.,* 2011, **23**, 2370–2380.
34 H. Jiang, J. Q. Hu, F. Gu and C. Z. Li, *J. Phys. Chem. C*, 2008, **112**, 12138–12141.
35 K. K. Jena, T. K. Rout, R. Narayan, K. V. S. N. Raju, *Polym. Int.*, 2012, **61**, 1101–1106.
36 L. C. Xu, J. M. Pan, Q. F. Xia, F. F.Shi, J. D. Dai, X. Wei and Y. S. Yan, *J. Phys. Chem. C*, 2012, **116**, 25309–25318.
37 X. M. Hou, L. X. Wang and J. C. Hao, *Mater. Lett.*, 2013, **107**, 162–165.
38 Z. L. Gong, D. Y. Tang and Y. D. Guo, *J. Mater. Chem.*, 2012, **22**, 16872–16879.
39 C. J. Chang and E. H. Kuo, *Thin Solid Films*, 2010, **519**, 1755–1760.
40 P. Pasetto, H. Blas, F. Audouin, C. Boissière, C. Sanchez, M. Save, B. Charleux, *Macromolecules*, 2009, **42**, 5983–5995.
41 T. Wu, Y. F. Zhang, X. F. Wang, S. Y. Liu, *Chem. Mater.*, 2008, **20**, 101–109.
42 L. C. Tan, J. Liu, W. H. Zhou, J. C. Wei and Z. P. Peng, *Mater. Sci. Eng., C*, 2014, **45**, 524–529.
43 M. Chen, M. Dong, R. Havelund, V. R. Regina, R. L. Meyer, F. Besenbacher, P. Kingshott, *Chem. Mater.*, 2010, **22**, 4214–4221.

Scheme 1

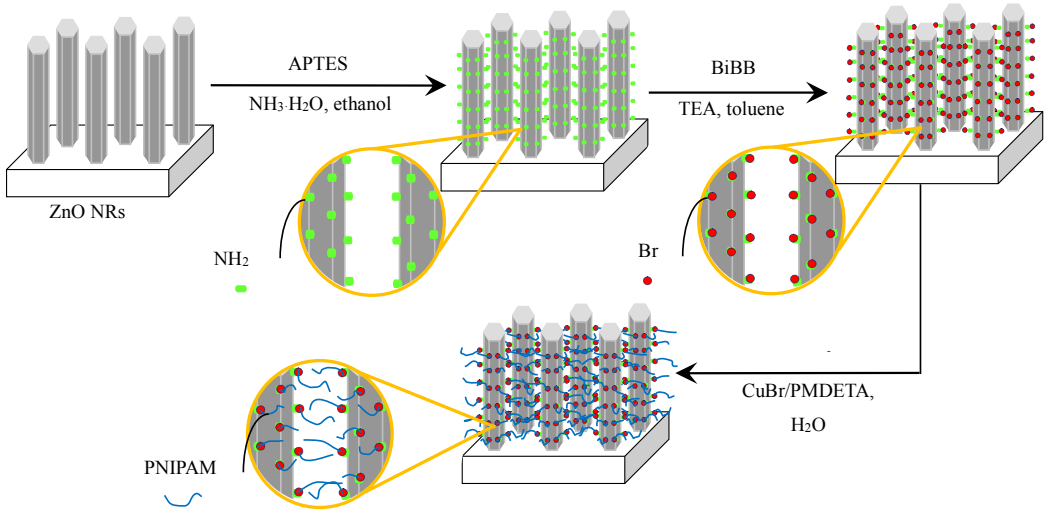

Scheme 2

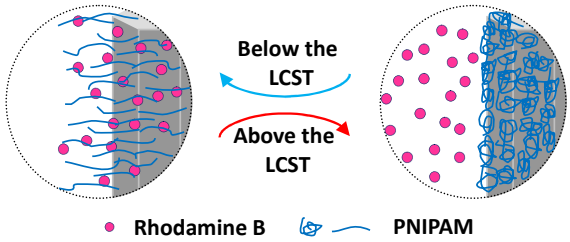

Fig. 1

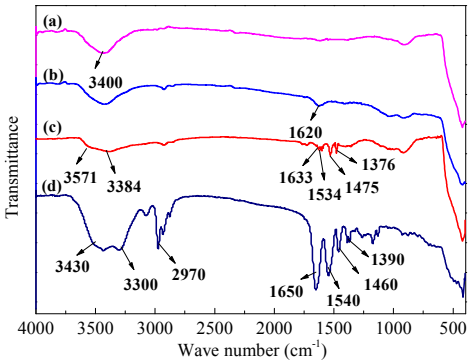

Fig. 2

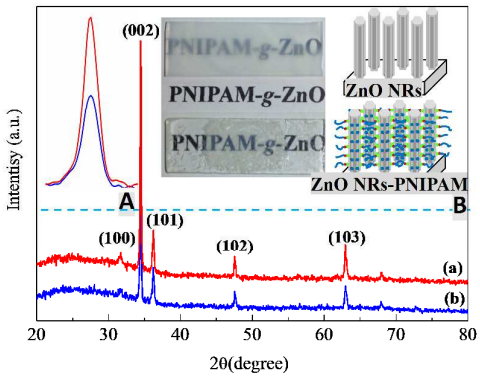

Fig. 3

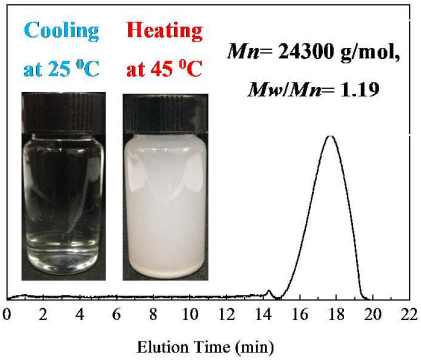

Fig. 4

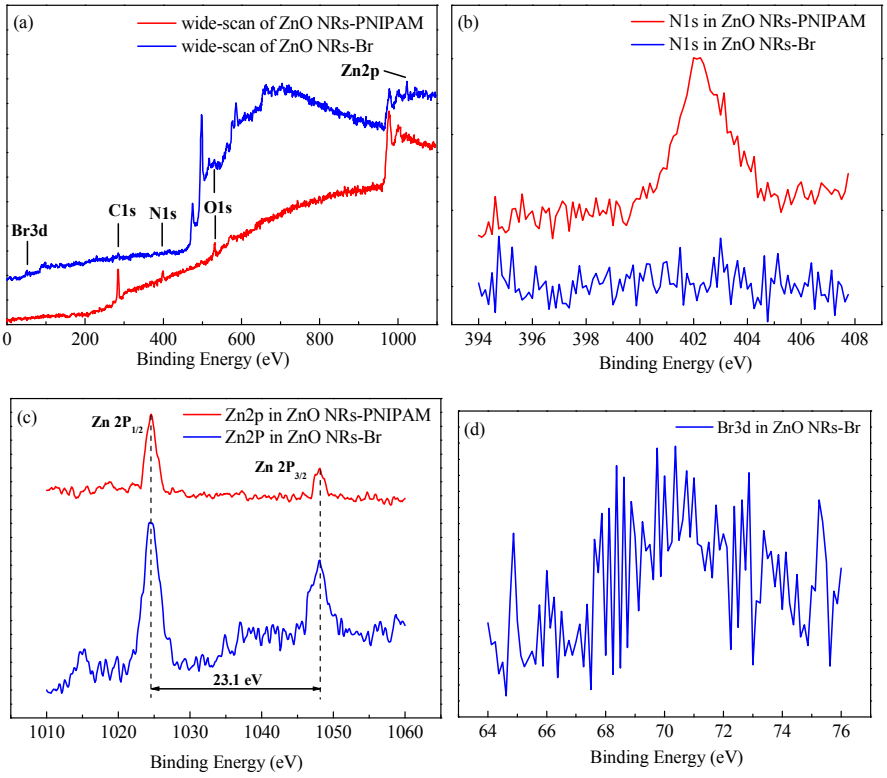

Fig. 5

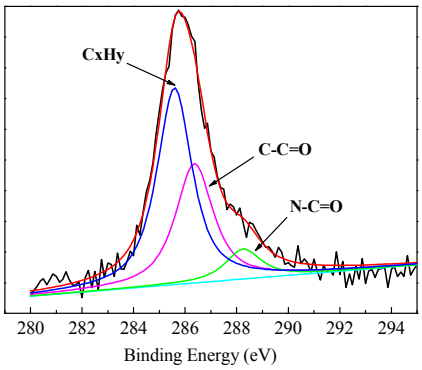

Fig. 6

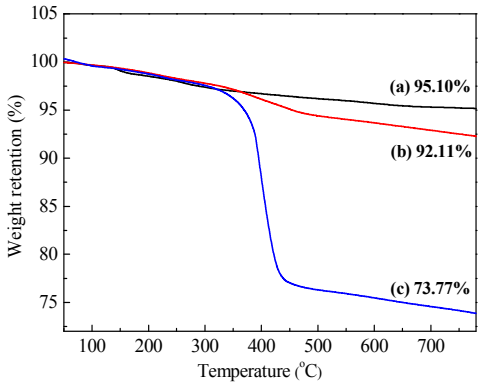

Fig. 7

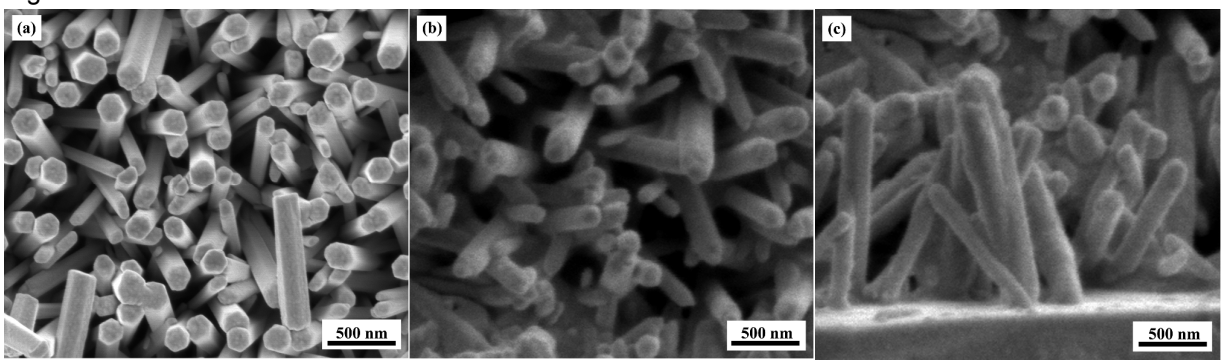

Fig. 8

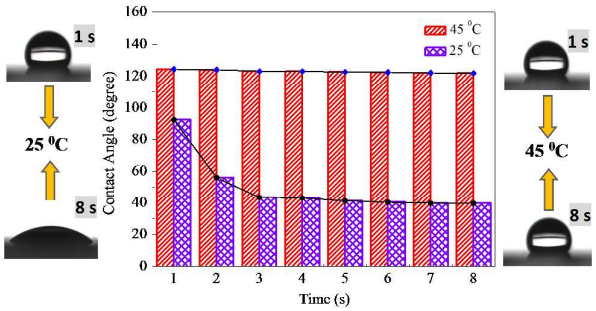

Fig. 9

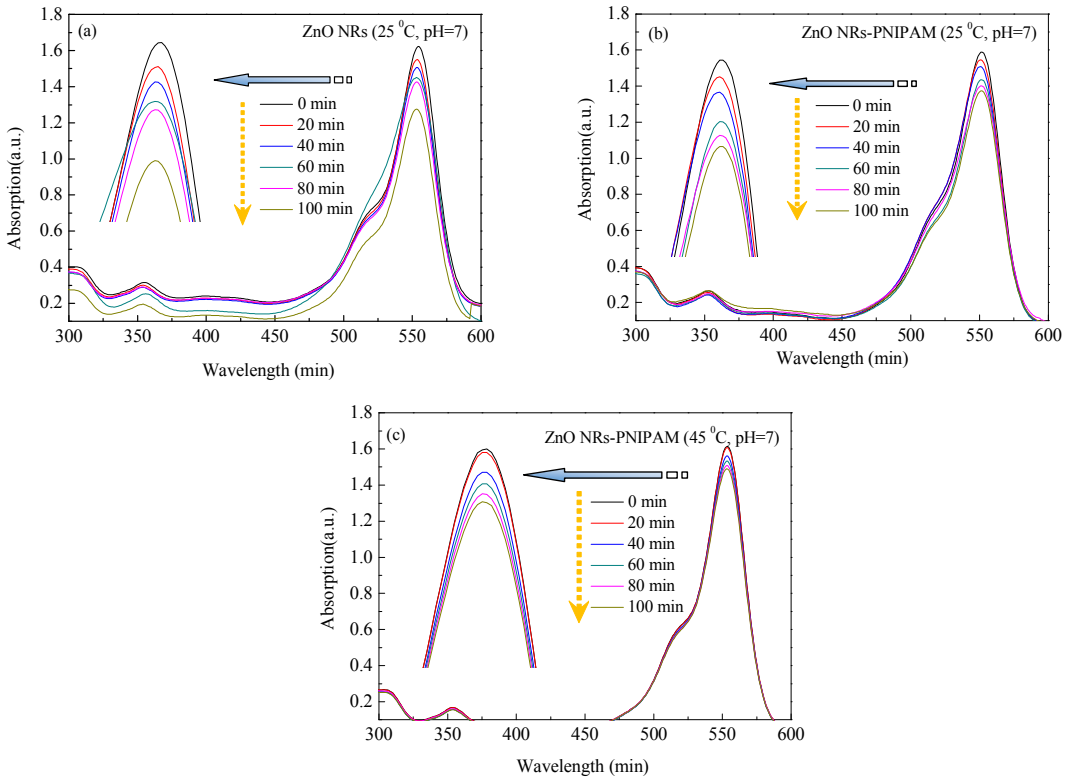

Fig. 10

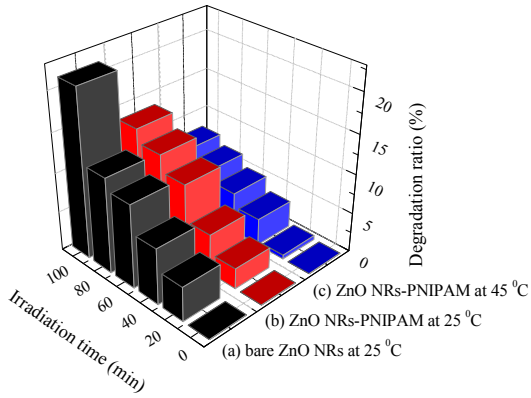

Table 1

Atomic Concentration					
Samples	C (%)	N (%)	O (%)	Zn (%)	Br (%)
ZnO NRs-Br	35.04	1.13	19.14	9.40	2.09
ZnO NRs-PNIPAM	78.16	8.77	9.83	2.24	0.00

Figure captions

Scheme 1 Illustration of the procedures of the preparation of ZnO NRs-PNIPAM by SI-ATRP.

Scheme 2 Illustration of the temperature-dependent photodegration of Rhodamine B with the expanded/collapsed polymer below/above the LCST, thus exposed/blocked the active sites.

Fig. 1 Fourier transform infrared (FT-IR) spectra of modified ZnO NRs at various stages: unmodified (a), –Amino (b), –BiBB (c), and –PNIPAM (d) grafted by SI-ATRP.

Fig. 2 XRD patterns of ZnO NRs (a) and ZnO NRs-PNIPAM (b) nanocomposites. (The insets of A were the peaks of NRs and nanocomposites located at (002) plane at a higher magnification. The left side of the insets of B were the optical photos of NRs and nanocomposites; the right side of the insets of B were the according schematic illustrations of NRs and nanocomposites.)

Fig. 3 Evolution of GPC traces with polymerization time and temperature during the SI-ATRP of NIPAM from ZnO NRs at 25 ^{0}C for 6 hours. PNIPAM was cleaved from ZnO NRs via etching with hydrofluoric acid. (The insets were the optical photos of PNIPAM cleaved from ZnO NRs in a clear or turbid state by cooling at 25 ^{0}C or heating at 45 ^{0}C).

Fig. 4 XPS spectra of ZnO NRs-Br and ZnO NRs-PNIPAM: wide-scan (a), N1s (b), Zn2p (c), and Br3d (d).

Fig. 5 C1s curve fitting spectrum of ZnO NRs-PNIPAM.

Fig. 6 TGA analysis of ZnO NRs (a), ZnO NRs-BiBB (b) and ZnO-NRs-PNIPAM (c).

Fig. 7 SEM images of top-view of ZnO NRs (a), top-view (b) and side-view (c) of ZnO NRs-PNIPAM.

Fig. 8 The surface contact angles of ZnO NRs-PNIPAM at 25 and 45 ^{0}C within 8 s. (The left side of the insets were the optical images of the surface contact angles of nanocomposites at 25 ^{0}C in 1 and 8 s and the right side of the inserts were those at 45 ^{0}C in 1 and 8 s.)

Fig. 9 UV-vis absorption spectra of Rh-B undergoing photodegradation in the present of ZnO NRs (a); and ZnO NRs-PNIPAM nanocomposites at 25 ^{0}C (b) and at 45 ^{0}C (c). (The insets were the curves of UV-vis absorption spectra at higher magnification).

Fig. 10 Degradation percentage of Rh-B solutions in the presence of ZnO NRs (a) and ZnO NRs-PNIPAM at 25 ^{0}C (b) and 45 ^{0}C (c) for 100 min, respectively.

Table 1 Atomic concentration of ZnO NRs-Br and ZnO NRs-PNIPAM calculated by XPS detection results.